12-5-2022

# Stiffness and Strain Properties Derived From Digital Tomosynthesis-Based Digital Volume Correlation Predict Vertebral Strength Independently From Bone Mineral Density

Yener N. Yeni

Daniel Oravec

Joshua Drost

Roger Zauel

Michael J. Flynn

**Yener N. Yeni**[1]
Mem. ASME
Bone & Joint Center,
Henry Ford Hospital Integrative Biosciences
Center (iBio),
6135 Woodward,
Detroit, MI 48202
e-mail: yeni@bjc.hfh.edu

**Daniel Oravec**
Bone & Joint Center,
Henry Ford Hospital Integrative Biosciences
Center (iBio),
6135 Woodward,
Detroit, MI 48202
e-mail: doravec1@hfhs.org

**Joshua Drost**
Bone & Joint Center,
Henry Ford Hospital Integrative Biosciences
Center (iBio),
6135 Woodward,
Detroit, MI 48202
e-mail: jdrost1@hfhs.org

**Roger Zauel**
Bone & Joint Center,
Henry Ford Hospital Integrative Biosciences
Center (iBio),
6135 Woodward,
Detroit, MI 48202
e-mail: rzauel@yahoo.com

**Michael J. Flynn**
Department of Radiology,
Henry Ford Hospital,
One Ford Place, Suite 2F,
Detroit, MI 48202
e-mail: mikef@rad.hfh.edu

# Stiffness and Strain Properties Derived From Digital Tomosynthesis-Based Digital Volume Correlation Predict Vertebral Strength Independently From Bone Mineral Density

*Vertebral fractures are the most common osteoporotic fractures, but their prediction using standard bone mineral density (BMD) measurements from dual energy X-ray absorptiometry (DXA) is limited in accuracy. Stiffness, displacement, and strain distribution properties derived from digital tomosynthesis-based digital volume correlation (DTS-DVC) have been suggested as clinically measurable metrics of vertebral bone quality. However, the extent to which these properties correlate to vertebral strength is unknown. To establish this relationship, two independent experiments, one examining isolated T11 and the other examining L3 vertebrae within the L2–L4 segments from cadaveric donors were utilized. Following DXA and DTS imaging, the specimens were uniaxially compressed to fracture. BMD, bone mineral content (BMC), and bone area were recorded for the anteroposterior and lateromedial views from DXA, stiffness, endplate to endplate displacement and distribution statistics of intravertebral strains were calculated from DTS-DVC and vertebral strength was measured from mechanical tests. Regression models were used to examine the relationships of strength with the other variables. Correlations of BMD with vertebral strength varied between experimental groups ($R^2_{adj} = 0.19–0.78$). DTS-DVC derived properties contributed to vertebral strength independently from BMD measures (increasing $R^2_{adj}$ to 0.64–0.95). DTS-DVC derived stiffness was the best single predictor ($R^2_{adj} = 0.66$, $p < 0.0001$) and added the most to BMD in models of vertebral strength for pooled T11 and L3 specimens ($R^2_{adj} = 0.95$, $p < 0.0001$). These findings provide biomechanical relevance to DTS-DVC calculated properties of vertebral bone and encourage further efforts in the development of the DTS-DVC approach as a clinical tool.* [DOI: 10.1115/1.4056196]

## Introduction

Vertebral fractures are the most common form of osteoporotic fractures [1–4] and have been associated with complications such as pulmonary [5,6] and gastroesophageal [7] problems as well as increased risk for further fractures [8–11]. Therefore, an accurate assessment of vertebral bone quality and risk of fracture is important for a timely intervention.

Currently, the standard clinical tool for diagnosing osteoporosis is dual energy X-ray absorptiometry (DXA), and DXA derived bone mineral density (BMD) is the most commonly referred metric for assessment of fracture risk. Though useful, DXA-based BMD is correlated to vertebral strength to an extent that varies from poor to excellent depending on the experiment [12–15], and has limited capacity to predict fracture risk [16]. Alternative approaches for estimating vertebral strength include finite element (FE) modeling using quantitative computed tomography, which has been successful in predicting vertebral strength [17–21]. However, due to radiation exposure concerns with computed tomography (CT), clinical FE applications are largely used in opportunistic screening utilizing existing CT scans. FE models also use assumptions on the material and loading conditions, which may result in errors if these assumptions substantially deviate from reality [22–24].

Digital volume correlation (DVC) was introduced as a powerful tool for studying three-dimensional (3D) strain distributions in complex structures such as cancellous bone using microcomputed tomography and mechanical loading [25]. Much has been learned about human vertebral bone mechanics by application of this method [26–29]. However, due to the nature of high powered imaging and ex-vivo mechanical loading, this technique remained largely as a laboratory tool and clinical applications of DVC did not emerge for axial skeleton of live humans until recently.

Digital tomosynthesis-based digital volume correlation (DTS-DVC) was introduced as a clinically feasible alternative for a direct biomechanics-based assessment of vertebral bone quality using deformation, stiffness, and strain measurements obtained under loading from the subject's body weight [30–32]. DTS is a cone beam tomography system that produces a stack of images of an object, which can be reconstructed as a 3D volume [33] (Fig. 1). DTS is able to acquire three-dimensional images of bones with low radiation exposure, about 12–17% of a CT scan [34,35]. Due to its versatility for scanning patients while they are lying or standing, the DTS scanner allows for pairing two sets of images

[1]Corresponding author.
Manuscript received May 25, 2022; final manuscript received October 31, 2022; published online December 5, 2022. Assoc. Editor: Sandra Shefelbine.

  

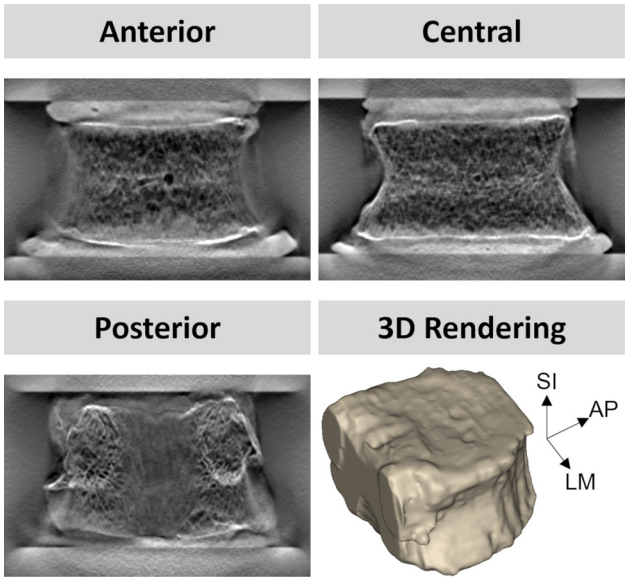


**Fig. 1 Representative coronal slices and 3D rendering from DTS reconstruction of a cadaveric T11 vertebra**

(one with patient's spine under load from body weight and one without) in a DVC application [30]. DTS images have high spatial resolution in the coronal or sagittal plane (approximately three times that of thin slice CT) [36], which facilitates calculation of deformations in the direction of major load transmission with DVC.

Displacement and stiffness measured from DTS-DVC have been shown to have a high correlation with those derived from microcomputed tomography ($\mu$CT) [31]. DTS-DVC derived strains generated under physiologically relevant loads have also been shown to have signal intensities sufficiently above background noise [32]. In addition, pilot studies showed that displacement derived from DTS-DVC is sensitive to increases in load bearing in vivo [30]. Together, these results suggest utility of DTS-DVC in the assessment of vertebral bone quality. However, the extent to which DTS-DVC parameters relate to vertebral strength is unknown. Without this information, it would be difficult to interpret the DTS derived metrics. Therefore, the goal of this work was to establish the extent to which DTS-DVC computed properties are associated with experimentally determined whole vertebral strength, alone and independently from BMD.

## Methods

All procedures described in this study were performed under the approval of Institutional Review Board. This study builds on a previous study that examined vertebral strains as measured from DTS-DVC using cadaveric vertebrae [32]. In the current study, the same specimens were subjected to mechanical testing to determine their strength, and the DXA and DTS images were further analyzed to derive additional BMD, displacement, and stiffness variables as described below. Two separate experiments were conducted, one utilizing isolated T11 vertebrae and the other utilizing L2–L4 segments from human cadavers. Though the experiments were considered separate, pooling was also explored when possible to determine the extent to which the findings could be generalizable over the range of conditions represented in the two experiments. Cadaveric specimens were wrapped in saline-soaked towels and stored at –20 C until experimental activities.

**Experiment 1: Isolated T11 Vertebral Bodies.** Eleven human cadaveric T11 vertebrae (5 F, 5 M; 62–96 yrs old) were utilized. The vertebrae were cleared of soft tissue and posterior processes were resected flush to the posterior cortex using a bone saw before imaging studies.

Isolated T11 vertebral bodies were imaged using a standard clinical DXA system with a fast array protocol in anteroposterior (AP) and lateromedial (LM) orientations (Discovery A, Hologic Inc., Marlborough, MA). During imaging, specimens were submerged in 0.9% saline. For each scanning orientation, areal BMD, BMC, and vertebral area ($BMD_{AP}$ and $BMD_{LM}$; $BMC_{AP}$ and $BMC_{LM}$ and $A_{AP}$ and $A_{LM}$, respectively) were recorded.

Following DXA imaging, endplates of T11 specimens were potted using a stiff polymeric filler (Bondo Corp, Atlanta, GA) to ensure flat boundary conditions for mechanical testing. Prepared specimens were aligned between platens in a custom radiolucent loader and DTS imaged (Sonialvision Safire II, Shimadzu Co., Kyoto, Japan) in a nonloaded state. Specimens were imaged again under 444.82 N load (100 lb), representing upper body weight of a typical human [37]. Before imaging, the load was held for 10 min to allow the displacement to stabilize. For all specimens, images were acquired at 75 kV with a tube current of 160 mA. Seventy-four projection images were acquired over a 40-deg arc and at a rate of 15 per second with 12 ms exposure per pulse. This is the typical DTS imaging protocol used in the clinic and corresponds to a radiation exposure that is approximately 15% of a CT scan [38]. Coronal planes were reconstructed at $0.28 \times 0.28$ mm pixel spacing with 1 mm slice thickness. Image volumes were resampled to isotropic voxel size using bicubic interpolation before DVC analysis.

Pairs of nonloaded and loaded images were coregistered at the inferior endplate to align the images for DVC (MIPAV, NIH, Bethesda, MD). Using the registered image pairs, reference point displacements were calculated using a custom DVC code [26,31]. In short, the DVC algorithm compares gray values surrounding each point in the unloaded volume to those in the loaded volume so as to optimize the sum of squared differences in density between corresponding voxels. From the full field displacement solution, the median endplate-to-endplate displacement was derived ($D_{DVC}$) [31]. The stiffness of each vertebra ($S_{DVC}$) was calculated by normalizing $D_{DVC}$ with applied load (Eq. (1))

$$S_{DVC} = \frac{\text{Load}}{D_{DVC}} = \frac{444.82}{D_{DVC}} \tag{1}$$

From displacements at each reference point throughout the vertebral body (630,975–1,284,058 points), axial strain (supero-inferior, $\varepsilon_{zz}$), maximum-magnitude principal strain ($\varepsilon_{max}$), maximum compressive and tensile principal strains ($\varepsilon_C$ and $\varepsilon_T$), and von Mises equivalent strain ($\varepsilon_{VM}$) were calculated. The distributions of intravertebral strains were previously noted to be non-normal [32]. Therefore, the volumetric median (MED), interquartile range (IQR), and nonparametric coefficient of variation (NCV) were calculated as measures of central, dispersion, and relative dispersion characteristics of the distributions for each strain type as described previously [32].

Following DTS imaging, T11 vertebral bodies, while still potted in the filler, were placed between metal platens and compressed to failure in a materials test machine (model 8501, Instron Corporation, Canton, MA). The vertebral bodies were preconditioned by quickly loading to 100 N at a rate of 10 N/s, and holding for 60 s. The specimens were then loaded to failure under displacement control at a rate corresponding to a nominal strain rate of 0.1%/s. Vertebral strength ($F_{max}$), was recorded as the maximum load on the force–displacement curve.

**Experiment 2: L2–L4 Vertebral Segments.** Thirteen L2–L4 vertebral segments (5 F, 7 M, one unknown; 51–75 yrs old) were utilized. The segments were cleared of surrounding soft tissue with ligaments, intervertebral disks, and posterior elements left intact.

L2–L4 vertebral segments were imaged using a fast array DXA protocol in AP and LM orientations (Hologic Discovery A).

During imaging, specimens were submerged in 0.9% saline. For the central vertebra in each segment (L3), $BMD_{AP}$, $BMD_{LM}$, $BMC_{AP}$, $BMC_{LM}$, $A_{AP}$ and $A_{LM}$ were recorded.

Following DXA imaging, posterior elements were resected from all vertebrae in the segment. The levels bounding L3 (L2 and L4) were cut using a precision diamond bandsaw (Model E300, Exakt, Oklahoma City, OK) to obtain 10 mm thick sections with parallel surface planes which were embedded in poly(methyl methacrylate). Specimens were constantly irrigated with 0.9% saline throughout preparation.

The embedded ends of the bounding vertebrae were aligned between radiolucent platens in the loader and each specimen was DTS imaged as described for T11 vertebrae. For the central L3 vertebra, displacement, stiffness, and strain parameters were calculated as described for T11 vertebrae, with 630,975–1,768,241 reference points [32].

Following DTS imaging, L2–L4 vertebral segments were placed between metal platens and a 250 N preload was applied at a rate of 10 N/s which was held for 60 s [39]. Constructs were then loaded to failure at a rate of 0.1 mm/s and vertebral strength was derived from the load–displacement data [40].

**Statistical Analysis.** The relationships between DTS parameters and $F_{max}$ were examined using linear regression and multiple linear regression. First, the relationships were examined separately in each experiment. Then, the relationship of a variable with vertebral strength was examined using the pooled data in a multiple regression model that included the variable of interest, experiment, and their interaction as independent variables. If both the experiment effect and the interaction were nonsignificant, then the variable was considered suitable for inclusion in subsequent models utilizing pooled data.

Multiple linear regression models of vertebral strength were then constructed using DTS-DVC and BMD properties. One group of models was constructed by forcing a BMD variable, in order to determine the extent to which DTS-DVC properties contribute to vertebral strength independently from BMD. Another group of models included only DTS-DVC variables in order to determine the extent to which DTS-DVC alone can explain vertebral strength.

Multiple regression models were constructed using a forward stepwise procedure. Models with high multicollinearity were dismissed based on a variance inflation factor criterion (VIF > 5). $D_{DVC}$ was not allowed in the same model with $S_{DVC}$, and NCV variables were not allowed in the same model with their respective MED or IQR variables, due to their arithmetic relationship with each other. In order to minimize overfitting, models with more than two independent variables were not considered for reporting. Significance was considered as $p < 0.05$. All analyses were performed in JMP (v10.0, SAS Institute, Inc., Cary, NC).

## Results

**Isolated T11 Vertebral Bodies.** In terms of DXA derived metrics, BMD and BMC measured from AP or lateral views were significantly positively correlated with strength for isolated T11 vertebrae, while the correlations of vertebral area from AP or lateral views were not significant (Table 1).

In terms of DTS derived metrics, significant positive correlations of $S_{DVC}$ and MED $\varepsilon_{zz}$ and a marginally significant negative correlation of $D_{DVC}$ with strength were found (Table 2). All other DTS derived metrics were nonsignificant.

In multiple regression models with $BMD_{AP}$ forced into the model, MED $\varepsilon_{max}$ and MED $\varepsilon_{VM}$ contributed to strength, independently from $BMD_{AP}$ (Table 3). With $BMD_{LM}$ forced in to the model instead of $BMD_{AP}$, DTS derived variables did not contribute further. Multiple regression models constructed using only DTS variables were not significant.

**L3 Vertebrae in L2–L4 Segments.** In contrast to the isolated T11 vertebrae, all DXA derived metrics, except for BMD from the AP view, were significantly positively correlated with strength for the L2–L4 segments (Table 1). The correlation of BMD from the AP view with strength was also positive, but only marginally significant (Table 1).

Similar to the case of T11 vertebrae, $S_{DVC}$, $D_{DVC}$, and MED $\varepsilon_{zz}$ were significantly correlated with strength for L2–L4 segments (Table 2). In addition, heterogeneity of the axial strain (IQR $\varepsilon_{zz}$) had a significant negative relationship with strength for the L2–L4 segments (Table 2).

Because $BMD_{LM}$ was a significant correlate of strength for the L2–L4 group and $BMD_{AP}$ was not, multiple regression models were constructed forcing $BMD_{LM}$ into the models. In this case, $S_{DVC}$, $D_{DVC}$, and MED $\varepsilon_{zz}$ contributed to strength independently from BMD (Table 4). When multiple regression models were constructed using only DTS variables, a model constructed using $D_{DVC}$ and NCV $\varepsilon_C$ was significant (Table 2).

**Combined T11 Vertebrae and L2–L4 Segments.** Pooling of the two groups of vertebrae was not feasible for a majority of DXA derived variables, either due to a significant interaction term (indicating different slopes) or a significant group effect (indicating different intercepts) in multiple regression models of strength (Table 1). BMD and area from the lateral view were the only DXA derived variables that passed this test, albeit marginally for the group effect ($p = 0.053$ and $p = 0.074$, respectively). When specimens from both experiments were pooled, vertebral strength was significantly correlated with $A_{LM}$ and $BMD_{LM}$ (Table 1, Fig. 2).

Pooling of the data for regressions of strength was feasible for a majority of DTS derived variables, including $D_{DVC}$, $S_{DVC}$, MED $\varepsilon_{zz}$, and IQR $\varepsilon_{zz}$ that were found to be significant for T11 and/or L3 alone, based on nonsignificant interaction and group effects. The regressions of vertebral strength on these variables were also significant for the pooled data (Table 2), with the relationship of strength to $D_{DVC}$ presenting a possible nonlinear trend (Fig. 2).

Because $BMD_{LM}$ is less prone to the presence of posterior elements and was significant for both T11 an L3, it was used as the

**Table 1 Univariate relationships between vertebral strength and DXA derived variables for T11, L3 and, when feasible, for the pooled T11 and L3**

| | T11 only ($N = 11$) | | | L3 only ($N = 13$) | | | Pooled ($N = 24$) | | |
|---|---|---|---|---|---|---|---|---|---|
| Parameter | $R^2$ | $R^2_{adj}$ | $p$-value | $R^2$ | $R^2_{adj}$ | $p$-value | $R^2$ | $R^2_{adj}$ | $p$-value |
| AAP | 0.162 | 0.069 | 0.219 | 0.789 | 0.770 | <0.0001 | NA; $p_G < 0.04$ | | |
| $BMC_{AP}$ | 0.810 | 0.789 | <0.0002 | 0.607 | 0.571 | <0.002 | NA; $p_G < 0.003$; $p_x < 0.03$ | | |
| $BMD_{AP}$ | 0.805 | 0.784 | <0.0002 | 0.284 | 0.219 | 0.060 | NA; $p_G < 0.05$ | | |
| ALM | 0.271 | 0.190 | 0.100 | 0.655 | 0.624 | <0.0009 | 0.467 | 0.443 | 0.0002 |
| $BMC_{LM}$ | 0.821 | 0.801 | <0.0002 | 0.791 | 0.772 | <0.0005 | NA; $p_x < 0.0007$ | | |
| $BMD_{LM}$ | 0.768 | 0.742 | <0.0005 | 0.597 | 0.561 | <0.002 | 0.599 | 0.580 | <0.0001 |

Models that are nonsignificant ($p > 0.05$) or not feasible for pooling have been shaded gray, based on a significant group ($p_G$) or interaction ($p_x$) in the full-factorial model. All reported relationships are positive.

**Table 2 Univariate relationships between vertebral strength and DTS derived variables for T11, L3 and, when feasible, for the pooled T11 and L3**

| | T11 only ($N = 11$) | | | L3 only ($N = 13$) | | | Pooled ($N = 24$) | | |
|---|---|---|---|---|---|---|---|---|---|
| Parameter | $R^2$ | $R^2_{adj}$ | $p$-value | $R^2$ | $R^2_{adj}$ | $p$-value | $R^2$ | $R^2_{adj}$ | $p$-value |
| DDVC (–) | 0.321 | 0.246 | 0.069 | 0.465 | 0.416 | <0.02 | 0.447 | 0.422 | <0.0004 |
| SDVC (+) | 0.465 | 0.406 | <0.03 | 0.695 | 0.668 | <0.0004 | 0.670 | 0.655 | <0.0001 |
| [a]MED $\varepsilon_{zz}$ (+) | 0.392 | 0.324 | <0.04 | 0.371 | 0.314 | <0.03 | 0.368 | 0.340 | <0.002 |
| IQR $\varepsilon_{zz}$ (–) | 0.137 | 0.041 | 0.262 | 0.369 | 0.312 | <0.03 | 0.286 | 0.254 | <0.008 |
| NCV $\varepsilon_{zz}$ (+) | 0.192 | 0.102 | 0.178 | 0.130 | 0.051 | 0.226 | 0.235 | 0.200 | <0.02 |

[a]Compressive direction is negative, i.e., strength decreases with increasing magnitude of MED $\varepsilon_{zz}$.
Included are variables for which the model was significant for at least one group (T11, L3, or pooled). Models that are nonsignificant ($p > 0.05$) for one group have been shaded gray. Those that are not significant for any group have not been included.

**Table 3 Multiple regression models including $BMD_{AP}$ and one DTS derived variable for T11**

| $R^2$ | $R^2_{adj}$ | Model | Est 1 | Est 2 | Est int | $p$-val 1 | $p$-val 2 | $p$-val int |
|---|---|---|---|---|---|---|---|---|
| 0.899 | 0.874 | $BMD_{AP} + MED\ \varepsilon_{max}$ | 7166 | –83,003 | 1617 | <0.0001 | <0.03 | <0.02 |
| 0.896 | 0.870 | $BMD_{AP} + MED\ \varepsilon_{VM}$ | 7145 | –197,044 | 1585 | <0.0001 | <0.03 | <0.03 |

Nonsignificant models have not been included. DTS derived variables were not significant when $BMD_{LM}$ was used in the multiple regression model. Est 1 means estimate for the first variable in the model, Est 2 means estimate for the second variable in the model, Est int means estimate for the intercept, $p$-val 1 means $p$-value for the first variable, $p$-val 2 means $p$-value for the second variable, and $p$-val int means $p$-value for the intercept.

**Table 4 Multiple regression models L3**

| $R^2$ | $R^2_{adj}$ | Model | Est 1 | Est 2 | Est int | $p$-val 1 | $p$-val 2 | $p$-val int |
|---|---|---|---|---|---|---|---|---|
| 0.957 | 0.948 | $BMD_{LM} + S_{DVC}$ | 4923 | 0.114 | –2461 | <0.0001 | <0.0001 | <0.0004 |
| 0.855 | 0.826 | $BMD_{LM} + D_{DVC}$ | 5808 | –66547 | 1039 | <0.0005 | <0.002 | 0.33 |
| 0.758 | 0.710 | $BMD_{LM}$ + [a]MED $\varepsilon_{zz}$ | 5860 | 1,628,329 | 635 | <0.003 | <0.03 | 0.64 |
| 0.706 | 0.647 | $D_{DVC}$ + NCV $\varepsilon_C$ | 147,224 | 6306 | 528 | <0.0008 | <0.02 | 0.79 |

[a]Compressive direction is negative, i.e., strength decreases with increasing magnitude of MED $\varepsilon_{zz}$.
Multiple regression models with $BMD_{AP}$ were not constructed as $BMD_{AP}$ was not correlated to strength for L3. Nonsignificant models have not been included. Est 1 means estimate for the first variable in the model, Est 2 means estimate for the second variable in the model, Est int means estimate for the intercept, $p$-val 1 means $p$-value for the first variable, $p$-val 2 means $p$-value for the second variable, and $p$-val int means $p$-value for the intercept.

**Table 5 Multiple regression models including $BMD_{LM}$ and one DTS derived variable for pooled T1 and L3**

| $R^2$ | $R^2_{adj}$ | Model | Est 1 | Est 2 | Est int | $p$-val 1 | $p$-val 2 | $p$-val int |
|---|---|---|---|---|---|---|---|---|
| 0.667 | 0.636 | $BMD_{LM} + D_{DVC}$ | 3622 | 30,464 | 2061 | <0.002 | <0.05 | <0.05 |
| 0.770 | 0.748 | $BMD_{LM} + S_{DVC}$ | 2596 | 0.088 | 139 | <0.007 | <0.0008 | 0.74 |
| 0.709 | 0.681 | $BMD_{LM}$ + IQR $\varepsilon_{zz}$ | 4218 | –690,241 | 2571 | <0.0001 | <0.02 | <0.01 |

Two-variable models with DTS derived variables only were not significant. Est 1 means estimate for the first variable in the model, Est 2 means estimate for the second variable in the model, Est int means estimate for the intercept, $p$-val 1 means $p$-value for the first variable, $p$-val 2 means $p$-value for the second variable, and $p$-val int means $p$-value for the intercept.

reference BMD parameter in multiple regression models of strength examining BMD-independent effects of DTS derived parameters in pooled data. In the pooled analyses, $D_{DVC}$, $S_{DVC}$, and IQR $\varepsilon_{zz}$ contributed to strength independently from $BMD_{LM}$, with the contribution increasing $R^2_{adj}$ values by 5.6–16.8% from those with $BMD_{LM}$ alone (Table 5, Fig. 3).

## Discussion

The goal of this work was to determine the extent to which DTS-DVC derived properties are associated with experimentally determined whole vertebral strength. We found that DTS-DVC derived displacement, stiffness, and strain variables significantly correlated to vertebral strength individually and independently from BMD.

Two different experiments were utilized representing a range of experimental approaches to vertebral strength testing in an attempt to identify commonalities in results. In general, DTS-DVC derived parameters were comparable between experiments, i.e., large differences in vertebral displacement, as would be expected in mechanical testing with very different interfaces between the load and the tested vertebra (the stiff polymeric filler versus the compliant intervertebral disk), did not occur between the experiments. This is largely because DVC can be used to calculate endplate-to-endplate displacements leaving out those occurring in the filler or the disk.

Within the range of variations imposed by the two experiments, stiffness appears to stand out among all DTS-DVC derived variables as a unifying property with its stronger relationship to strength than other DTS derived variables in both experiments, its ability to be pooled over two sets of data, and its contribution to strength independently from BMD providing the model with the highest explanatory capability for strength. In the pooled data it was also the most explanatory single predictor of strength. These findings are consistent with stiffness being perhaps the strongest correlate of vertebral strength that can be measured nondestructively [17,41].

The contribution of $S_{DVC}$ to strength in the presence of a BMD measure was different for T11 and L3. This may be due to the

strength versus BMD relationship itself being different between the isolated T11 and L3 segments. Strength had a strong correlation with both $BMD_{AP}$ and $BMD_{LM}$ in isolated T11 whereas these relationships were nonsignificant or more moderate in L3 segments, leaving more to explain in L3. Several previous studies utilizing a variety of experimental conditions found similar results: The relationship of strength to BMD is weaker at L2–L4 sites than at T11 [42], and weaker with $BMD_{AP}$ than with $BMD_{LM}$ for the lumbar sites [14,42–44]. Though the condition of fillers (disk or stiffer manmade polymers) may cause changes in strain distributions that have biological significance [45–47], they are less likely to affect the ability of stiffness to predict strength at a given instant [48–50]. As such, we believe the difference in correlations of strength with BMD between T11 and L3 is more intrinsic to the vertebral levels than can be attributable to the boundary conditions of the test. Thoracic 11 experiences more compressive loads than lumbar levels [51] and the T11 cancellous bone is more adapted to undertake uniaxial compressive loads in the direction of vertebral axis [52]. It is possible that due to such adaptations, structural information is better coupled with density in T11 than in L3, and addition of stiffness to BMD does not add further information in prediction of strength for T11. However, whereas L3 is included in standard clinical DXA examinations, T11 is not. In the absence of standard DXA capability for BMD measurements at thoracic levels, the DVC outcomes may have a more significant utility. Nonetheless, the findings that $S_{DVC}$ was the most explanatory single predictor, and together with $BMD_{LM}$ provided the most explanatory model of strength for the pooled data, are encouraging for further consideration of the DTS-DVC approach as a biomechanics-based evaluation of vertebral bone quality.

Not surprisingly, the reciprocal of overall displacement produced results similar to stiffness in this study. This is due to the fact that the measured displacement was generated under a load identical for all specimens. In an in vivo application, stiffness calculation would require some knowledge of patient-specific loads

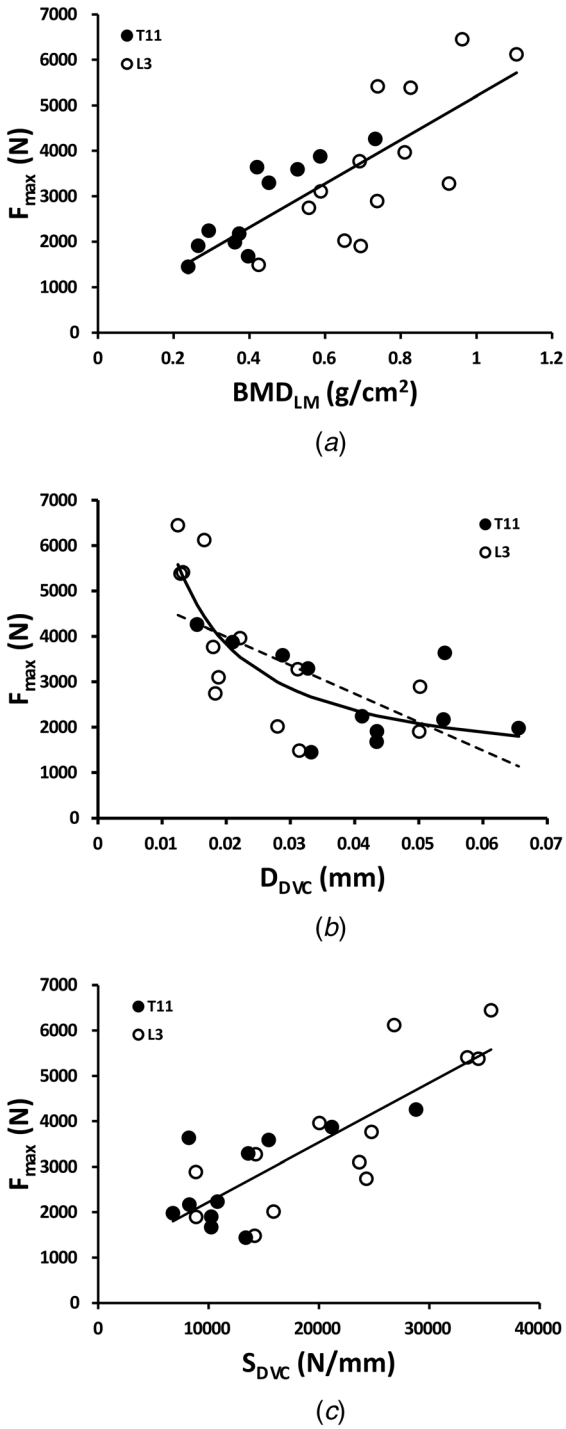


**Fig. 2** (*a*) BMD from lateral DXA positively correlated to vertebral strength for pooled T11 and L3 vertebrae: $F_{max} = 4818\ BMD_{LM} + 385$; $R^2 = 0.60$, $p < 0.0001$. (*b*) DTS-DVC derived displacement ($D_{DVC}$) negatively correlated to vertebral strength for pooled T11 and L3 vertebrae: $F_{max} = -62661\ D_{DVC} + 5245$ ($R^2 = 0.45$; $p < 0.0004$). A nonlinear fit was more explanatory: $F_{max} = 58.4\ (1/D_{DVC}) + 908.6$ ($R^2 = 0.67$; $p < 0.0001$). (*c*) DTS-DVC derived stiffness ($S_{DVC}$) positively correlated to vertebral strength for pooled T11 and L3 vertebrae: $F_{max} = 0.131\ S_{DVC} + 909$ ($R^2 = 0.67$; $p < 0.0001$).

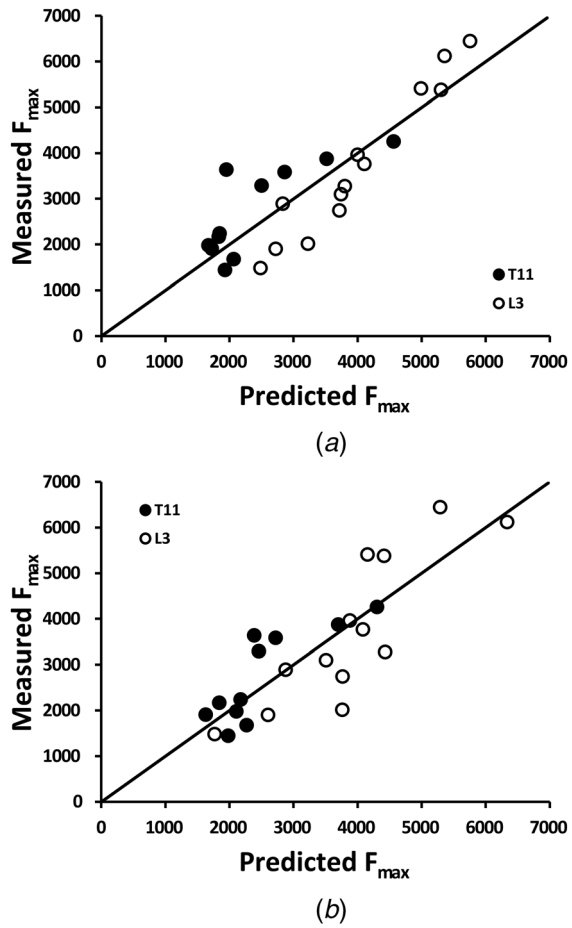


**Fig. 3** Multiple regression models of strength with (*a*) $BMD_{LM}$ and $S_{DVC}$, and (*b*) $BMD_{LM}$ and IQR $\varepsilon_{zz}$ as predictors increased explained variability by 17.1% and 11%, respectively (compare to Fig. 2(*a*)), for pooled T11 and L3

and the two variables would be differentiated from each other by this additional factor. As such, $D_{DVC}$ would serve as a composite parameter containing information intrinsic to the vertebra as well as the load levels while $S_{DVC}$ would represent qualities intrinsic to the vertebra. Both could be useful in understanding the extent to which a given vertebra is at risk of fracture; however, a comparison of the two variables can be more appropriately done in future in vivo studies where patient-specific loading can be taken into account.

Median strain in the direction of the vertebral axis (MED $\varepsilon_{zz}$) consistently correlated to strength for T11 alone, L3 alone, and pooled T11 and L3, while other strain variables did not exhibit a consistent trend. MED $\varepsilon_{zz}$ is expected to be correlated to the longitudinal displacement and stiffness, and thus have a similar relationship to strength. In addition, being in the direction of the applied load, $\varepsilon_{zz}$ might be expected to reach magnitudes that offer better signal relative to noise for DVC calculations. It is also the only strain, among those studied here, that is directly recorded from DVC without using calculations that involve low-resolution components of the strain tensor, i.e., those generated in lower magnitudes or in directions of low image resolution. As such, the persistent correlation of $\varepsilon_{zz}$ with strength may be due to resolution conditions being more favorable for measurement of $\varepsilon_{zz}$ than other strains. However, when used together with BMD measures, MED $\varepsilon_{zz}$ persisted as a significant predictor for L3 vertebrae only. As in the argument of $S_{DVC}$, this may be attributable to L3 mechanical properties being less attuned to BMD, leaving more to be explained by mechanical variables.

In general, strain measures were less explanatory than $S_{DVC}$ (analogously, reciprocal $D_{DVC}$) for strength. An exception was for isolated T11 vertebrae, where addition of MED $\varepsilon_{VM}$ or MED $\varepsilon_{max}$ to $BMD_{AP}$ was significant and increased $R^2_{adj}$ by 8.6–9%. These strains are often associated with failure of materials, and a decrease in strength with increasing values of these strains for a given BMD is consistent with this notion. However, observation of this effect for T11 alone and only after accounting for $BMD_{AP}$ suggests limited utility as a universal predictor of vertebral strength.

The limitations of the study must be recognized. Although performing this experiment using two different sets of vertebrae with different experimental conditions provides strength in terms of confirming and generalizing the findings, it also presents weaknesses. Due to inclusion of posterior elements in L3 DXA scans but not in T11 scans, a dichotomy in results involving $BMD_{AP}$ would be expected. For this reason, we could not pool the data for models involving $BMD_{AP}$, which is the standard BMD used in clinical practice. Instead, we used $BMD_{LM}$ which does not involve posterior elements. However, $BMD_{LM}$ is strongly correlated with $BMD_{AP}$ [14,53,54] and is expected to serve as a good surrogate for $BMD_{AP}$. Our goal was not exhaustively investigating DXA-based methods and as such some advanced DXA image analysis techniques were not explored (e.g., Ref. [55]). However, it should be noted that DXA derived variables, even from such advanced analyses, would still not be biomechanics based and as such would be out of scope in our search for biomechanics-based predictors of vertebral strength and fracture risk. Nonetheless, future studies should consider multiple vertebral levels using the same image and test protocol to establish more strongly the universality of DTS-DVC derived metrics over BMD.

Strains generated in the vertebra are obviously a function of the applied load, and it is possible that higher signal levels may be achieved under higher loads. Although we used a load of physiologically relevant magnitude for standing [37] in this experiment, and previously demonstrated that this load generates strains above noise levels [32], in vivo loads, may generate smaller or larger strains than obtained in this experiment in patient-specific applications.

In conclusion, the current data demonstrate that DTS-DVC derived stiffness and strain distribution properties of vertebral bone are correlated to vertebral strength independently from bone density, providing rationale for their use in biomechanics-based assessment of vertebral bone quality. The extent to which these metrics can improve prediction of vertebral fractures remains to be investigated in future in vivo studies.


## Acknowledgment

This project was supported by the National Institutes of Health under NIH Grant No. R21AR070363. Its contents are solely the responsibility of the authors and do not necessarily represent the official views of NIH.

## Funding Data

- National Institutes of Health NIH (Grant No. R21AR070363; Funder ID: 10.13039/100000002).


## Data Availability Statement

The datasets generated and supporting the findings of this article are obtainable from the corresponding author upon reasonable request.

## Nomenclature

$A_{AP}$ = area of the vertebra measured from anteroposterior projection DXA, $mm^2$
$A_{LM}$ = area of the vertebra measured from lateromedial projection DXA, $mm^2$
AP = anteroposterior direction
BMC = bone mineral content, g
$BMC_{AP}$ = bone mineral content measured in anteroposterior orientation, g
$BMC_{LM}$ = bone mineral content measured in lateromedial orientation, g
BMD = bone mineral density, $g/cm^2$
$BMD_{AP}$ = bone mineral density measured in anteroposterior orientation, $g/cm^2$
$BMD_{LM}$ = bone mineral density measured in lateromedial orientation, $g/cm^2$
CT = computed tomography
$D_{DVC}$ = digital volume correlation derived endplate-to-endplate displacement, mm
DTS-DVC = digital tomosynthesis-based digital volume correlation
DVC = digital volume correlation
DXA = dual X-ray absorptiometry
$F_{max}$ = maximum load on the force-displacement curve (vertebral strength)
FE = finite element
IQR = interquartile range
kV = kilovolts
lb = pounds
LM = lateromedial direction
L2–L4 = segment including second through fourth lumbar vertebrae
L3 = third lumbar vertebra
mA = milliamperes
MED = median
mm = millimeters
ms = milliseconds
N = Newtons
NCV = nonparametric coefficient of variation (IQR/MED)
$S_{DVC}$ = digital volume correlation derived stiffness, N/mm
T11 = 11th thoracic vertebra
VIF = variance inflation factor
$\varepsilon_C$ = maximum compressive strain
$\varepsilon_T$ = maximum tensile strain
$\varepsilon_{VM}$ = von Mises equivalent strain
$\varepsilon_{max}$ = maximum magnitude principal strain

$\varepsilon_{zz}$ = axial (superio-inferior) strain
$\mu$CT = microcomputed tomography

## References


[1] Samelson, E. J., Hannan, M. T., Zhang, Y., Genant, H. K., Felson, D. T., and Kiel, D. P., 2006, "Incidence and Risk Factors for Vertebral Fracture in Women and Men: 25-Year Follow-Up Results From the Population-Based Framingham Study," J. Bone Miner. Res., **21**(8), pp. 1207–1214.

[2] Felsenberg, D., Silman, A. J., Lunt, M., Armbrecht, G., Ismail, A. A., Finn, J. D., Cockerill, W. C., et alet al., 2002, "Incidence of Vertebral Fracture in Europe: Results From the European Prospective Osteoporosis Study (EPOS)," J. Bone Miner. Res., **17**(4), pp. 716–724.

[3] Burge, R., Dawson-Hughes, B., Solomon, D. H., Wong, J. B., King, A., and Tosteson, A., 2007, "Incidence and Economic Burden of Osteoporosis-Related Fractures in the United States, 2005-2025," J. Bone Miner. Res., **22**(3), pp. 465–475.

[4] Sambrook, P., and Cooper, C., 2006, "Osteoporosis," Lancet, **367**(9527), pp. 2010–2018.

[5] Di Bari, M., Chiarlone, M., Matteuzzi, D., Zacchei, S., Pozzi, C., Bellia, V., Tarantini, F., Pini, R., Masotti, G., and Marchionni, N., 2004, "Thoracic Kyphosis and Ventilatory Dysfunction in Unselected Older Persons: An Epidemiological Study in Dicomano, Italy," J. Am. Geriatr. Soc., **52**(6), pp. 909–915.

[6] Schlaich, C., Minne, H. W., Bruckner, T., Wagner, G., Gebest, H. J., Grunze, M., Ziegler, R., and Leidig-Bruckner, G., 1998, "Reduced Pulmonary Function in Patients With Spinal Osteoporotic Fractures," Osteoporosis Int., **8**(3), pp. 261–267.

[7] Miyakoshi, N., Kasukawa, Y., Sasaki, H., Kamo, K., and Shimada, Y., 2009, "Impact of Spinal Kyphosis on Gastroesophageal Reflux Disease Symptoms in Patients With Osteoporosis," Osteoporosis Int., **20**(7), pp. 1193–1198.

[8] Klotzbuecher, C. M., Ross, P. D., Landsman, P. B., Abbott, T. A., 3rd., and Berger, M., 2010, "Patients With Prior Fractures Have an Increased Risk of Future Fractures: A Summary of the Literature and Statistical Synthesis," J. Bone Miner. Res., **15**(4), pp. 721–739.

[9] Lindsay, R., Silverman, S. L., Cooper, C., Hanley, D. A., Barton, I., Broy, S. B., Licata, A., Benhamou, L., Geusens, P., Flowers, K., Stracke, H., and Seeman, E., 2001, "Risk of New Vertebral Fracture in the Year Following a Fracture," JAMA, **285**(3), pp. 320–323.

[10] Delmas, P. D., Genant, H. K., Crans, G. G., Stock, J. L., Wong, M., Siris, E., and Adachi, J. D., 2003, "Severity of Prevalent Vertebral Fractures and the Risk of Subsequent Vertebral and Nonvertebral Fractures: Results From the MORE Trial," Bone, **33**(4), pp. 522–532.

[11] Melton, L. J., 3rd, Atkinson, E. J., Cooper, C., O'Fallon, W. M., and Riggs, B. L., 1999, "Vertebral Fractures Predict Subsequent Fractures," Osteoporosis Int., **10**(3), pp. 214–221.

[12] Buckley, J. M., Cheng, L., Loo, K., Slyfield, C., and Xu, Z., 2007, "Quantitative Computed Tomography-Based Predictions of Vertebral Strength in Anterior Bending," Spine, **32**(9), pp. 1019–1027.

[13] Hulme, P. A., Boyd, S. K., and Ferguson, S. J., 2007, "Regional Variation in Vertebral Bone Morphology and Its Contribution to Vertebral Fracture Strength," Bone, **41**(6), pp. 946–957.

[14] Roux, J. P., Wegrzyn, J., Boutroy, S., Bouxsein, M. L., Hans, D., and Chapurlat, R., 2013, "The Predictive Value of Trabecular Bone Score (TBS) on Whole Lumbar Vertebrae Mechanics: An Ex Vivo Study," Osteoporosis Int., **24**(9), pp. 2455–2460.

[15] Ebbesen, E. N., Thomsen, J. S., Beck-Nielsen, H., Nepper-Rasmussen, H. J., and Mosekilde, L., 1999, "Lumbar Vertebral Body Compressive Strength Evaluated by Dual-Energy X-Ray Absorptiometry, Quantitative Computed Tomography, and Ashing," Bone, **25**(6), pp. 713–724.

[16] Cranney, A., Jamal, S. A., Tsang, J. F., Josse, R. G., and Leslie, W. D., 2007, "Low Bone Mineral Density and Fracture Burden in Postmenopausal Women," CMAJ, **177**(6), pp. 575–580.

[17] Crawford, R. P., Cann, C. E., and Keaveny, T. M., 2003, "Finite Element Models Predict In Vitro Vertebral Body Compressive Strength Better Than Quantitative Computed Tomography," Bone, **33**(4), pp. 744–750.

[18] Silva, M. J., Keaveny, T. M., and Hayes, W. C., 1998, "Computed Tomography-Based Finite Element Analysis Predicts Failure Loads and Fracture Patterns for Vertebral Sections," J. Orthop. Res., **16**(3), pp. 300–308.

[19] Liebschner, M. A., Kopperdahl, D. L., Rosenberg, W. S., and Keaveny, T. M., 2003, "Finite Element Modeling of the Human Thoracolumbar Spine," Spine, **28**(6), pp. 559–565.

[20] Imai, K., Ohnishi, I., Bessho, M., and Nakamura, K., 2006, "Nonlinear Finite Element Model Predicts Vertebral Bone Strength and Fracture site," Spine (Phila Pa 1976), **31**(16), pp. 1789–1794.

[21] Buckley, J. M., Loo, K., and Motherway, J., 2007, "Comparison of Quantitative Computed Tomography-Based Measures in Predicting Vertebral Compressive Strength," Bone, **40**(3), pp. 767–774.

[22] Aiyangar, A. K., Vivanco, J., Au, A. G., Anderson, P. A., Smith, E. L., and Ploeg, H. L., 2014, "Dependence of Anisotropy of Human Lumbar Vertebral Trabecular Bone on Quantitative Computed Tomography-Based Apparent Density," ASME J. Biomech. Eng., **136**(9), p. 091003.

[23] Erdem, I., Truumees, E., and van der Meulen, M. C., 2013, "Simulation of the Behaviour of the L1 Vertebra for Different Material Properties and Loading Conditions," Comput. Methods Biomech. Biomed. Eng., **16**(7), pp. 736–746.

[24] Yerby, S. A., Bay, B. K., Toh, E., McLain, R. F., and Drews, M. J., 1998, "The Effect of Boundary Conditions on Experimentally Measured Trabecular Strain in the Thoracic Spine," J. Biomech., **31**(10), pp. 891–897.

[25] Bay, B. K., Smith, T. S., Fyhrie, D. P., and Saad, M., 1999, "Digital Volume Correlation: Three-Dimensional Strain Mapping Using X-Ray Tomography," Exp. Mech., **39**(3), pp. 217–226.

[26] Zauel, R., Yeni, Y. N., Bay, B. K., Dong, X. N., and Fyhrie, D. P., 2006, "Comparison of the Linear Finite Element Prediction of Deformation and Strain of Human Cancellous Bone to 3D Digital Volume Correlation Measurements," ASME J. Biomech. Eng., **128**(1), pp. 1–6.

[27] Liu, L., and Morgan, E. F., 2007, "Accuracy and Precision of Digital Volume Correlation in Quantifying Displacements and Strains in Trabecular Bone," J. Biomech., **40**(15), pp. 3516–3520.

[28] Hussein, A. I., and Morgan, E. F., 2013, "The Effect of Intravertebral Heterogeneity in Microstructure on Vertebral Strength and Failure Patterns," Osteoporosis Int., **24**(3), pp. 979–989.

[29] Palanca, M., Cristofolini, L., Dall'Ara, E., Curto, M., Innocente, F., Danesi, V., and Tozzi, G., 2016, "Digital Volume Correlation Can Be Used to Estimate Local Strains in Natural and Augmented Vertebrae: An Organ-Level Study," J. Biomech., **49**(16), pp. 3882–3890.

[30] Oravec, D., Flynn, M. J., Zauel, R., Rao, S., and Yeni, Y. N., 2019, "Digital Tomosynthesis Based Digital Volume Correlation: A Clinically Viable Noninvasive Method for Direct Measurement of Intravertebral Displacements Using Images of the Human Spine Under Physiological Load," Med. Phys., **46**(10), pp. 4553–4562.

[31] Oravec, D., Zauel, R., Flynn, M. J., and Yeni, Y. N., 2020, "Vertebral Stiffness Measured Via Tomosynthesis-Based Digital Volume Correlation is Strongly Correlated With Reference Values From micro-CT-Based DVC," Med. Eng. Phys., **84**, pp. 169–173.

[32] Oravec, D., Drost, J., Zauel, R., Flynn, M. J., and Yeni, Y. N., 2021, "Assessment of Intravertebral Mechanical Strains and Cancellous Bone Texture Under Load Using a Clinically Available Digital Tomosynthesis Modality," ASME J. Biomech. Eng., **143**(10), p. 101011.

[33] Dobbins, J. T., 3rd., and Godfrey, D. J., 2003, "Digital x-Ray Tomosynthesis: Current State of the Art and Clinical Potential," Phys. Med. Biol., **48**(19), pp. R65–R106.

[34] Mettler, F. A., Jr., Huda, W., Yoshizumi, T. T., and Mahesh, M., 2008, "Effective Doses in Radiology and Diagnostic Nuclear Medicine: A Catalog," Radiology, **248**(1), pp. 254–263.

[35] Zhang, Y., Li, X., Segars, W. P., and Samei, E., 2014, "Comparison of Patient Specific Dose Metrics Between Chest Radiography, Tomosynthesis, and CT for Adult Patients of Wide Ranging Body Habitus," Med. Phys., **41**(2), p. 023901.

[36] Flynn, M. J., McGee, R., and Blechinger, J., 2007, "Spatial Resolution of X-Ray Tomosynthesis in Relation to Computed Tomography for Coronal/Sagittal Images of the Knee," SPIE Paper No. 65100D.

[37] Iyer, S., Christiansen, B. A., Roberts, B. J., Valentine, M. J., Manoharan, R. K., and Bouxsein, M. L., 2010, "A Biomechanical Model for Estimating Loads on Thoracic and Lumbar Vertebrae," Clin. Biomech. (Bristol, Avon), **25**(9), pp. 853–858.

[38] Oravec, D., Yaldo, O., Bolton, C., Flynn, M. J., van Holsbeeck, M., and Yeni, Y. N., 2019, "Digital Tomosynthesis and Fractal Analysis Predict Prevalent Vertebral Fractures in Patients With Multiple Myeloma: A Preliminary In Vivo Study," AJR Am. J. Roentgenol., **213**(1), pp. W38–W44.

[39] Wagnac, E., Aubin, C. E., Chaumoitre, K., Mac-Thiong, J. M., Menard, A. L., Petit, Y., Garo, A., and Arnoux, P. J., 2017, "Substantial Vertebral Body Osteophytes Protect Against Severe Vertebral Fractures in Compression," PLoS One, **12**(10), p. e0186779.

[40] Lu, Y., Krause, M., Bishop, N., Sellenschloh, K., Gluer, C. C., Puschel, K., Amling, M., Morlock, M. M., and Huber, G., 2015, "The Role of Patient-Mode High-Resolution Peripheral Quantitative Computed Tomography Indices in the Prediction of Failure Strength of the Elderly Women's Thoracic Vertebral Body," Osteoporosis Int., **26**(1), pp. 237–244.

[41] Chevalier, Y., Charlebois, M., Pahr, D., Varga, P., Heini, P., Schneider, E., and Zysset, P., 2008, "A Patient-Specific Finite Element Methodology to Predict Damage Accumulation in Vertebral Bodies Under Axial Compression, Sagittal Flexion and Combined Loads," Comput. Methods Biomech. Biomed. Eng., **11**(5), pp. 477–487.

[42] Moro, M., Hecker, A. T., Bouxsein, M. L., and Myers, E. R., 1995, "Failure Load of Thoracic Vertebrae Correlates With Lumbar Bone Mineral Density Measured by DXA," Calcif. Tissue Int., **56**(3), pp. 206–209.

[43] Myers, B. S., Arbogast, K. B., Lobaugh, B., Harper, K. D., Richardson, W. J., and Drezner, M. K., 2009, "Improved Assessment of Lumbar Vertebral Body Strength Using Supine Lateral Dual-Energy X-Ray Absorptiometry," J. Bone Miner. Res., **9**(5), pp. 687–693.

[44] Bjarnason, K., Hassager, C., Svendsen, O. L., Stang, H., and Christiansen, C., 1996, "Anteroposterior and Lateral Spinal DXA for the Assessment of Vertebral Body Strength: Comparison With Hip and Forearm Measurement," Osteoporosis Int., **6**(1), pp. 37–42.

[45] Eswaran, S. K., Gupta, A., and Keaveny, T. M., 2007, "Locations of Bone Tissue at High Risk of Initial Failure During Compressive Loading of the Human Vertebral Body," Bone, **41**(4), pp. 733–739.

[46] Jackman, T. M., DelMonaco, A. M., and Morgan, E. F., 2016, "Accuracy of Finite Element Analyses of CT Scans in Predictions of Vertebral Failure Patterns Under Axial Compression and Anterior Flexion," J. Biomech., **49**(2), pp. 267–275.

[47] Maquer, G., Schwiedrzik, J., Huber, G., Morlock, M. M., and Zysset, P. K., 2015, "Compressive Strength of Elderly Vertebrae is Reduced by Disc Degeneration and Additional Flexion," J. Mech. Behav. Biomed. Mater., **42**, pp. 54–66.

[48] Nekkanty, S., Yerramshetty, J., Kim, D. G., Zauel, R., Johnson, E., Cody, D. D., and Yeni, Y. N., 2010, "Stiffness of the Endplate Boundary Layer and Endplate Surface Topography Are Associated With Brittleness of Human Whole Vertebral Bodies," Bone, **47**(4), pp. 783–789.
[49] Kosmopoulos, V., Keller, T. S., and Schizas, C., 2009, "Early Stage Disc Degeneration Does Not Have an Appreciable Affect on Stiffness and Load Transfer Following Vertebroplasty and Kyphoplasty," Eur. Spine J., **18**(1), pp. 59–68.
[50] Buckley, J. M., Leang, D. C., and Keaveny, T. M., 2006, "Sensitivity of Vertebral Compressive Strength to Endplate Loading Distribution," ASME J. Biomech. Eng., **128**(5), pp. 641–646.
[51] Bruno, A. G., Burkhart, K., Allaire, B., Anderson, D. E., and Bouxsein, M. L., 2017, "Spinal Loading Patterns From Biomechanical Modeling Explain the High Incidence of Vertebral Fractures in the Thoracolumbar Region," J. Bone Miner. Res., **32**(6), pp. 1282–1290.
[52] Yeni, Y. N., Kim, D. G., Divine, G. W., Johnson, E. M., and Cody, D. D., 2009, "Human Cancellous Bone From T12-L1 Vertebrae Has Unique Microstructural and Trabecular Shear Stress Properties," Bone, **44**(1), pp. 130–136.
[53] Nicholson, P. H., and Alkalay, R., 2007, "Quantitative Ultrasound Predicts Bone Mineral Density and Failure Load in Human Lumbar Vertebrae," Clin. Biomech. (Bristol, Avon), **22**(6), pp. 623–629.
[54] Bjarnason, K., Nilas, L., Hassager, C., and Christiansen, C., 1995, "Dual Energy X-Ray Absorptiometry of the Spine–Decubitus Lateral Versus Anteroposterior Projection in Osteoporotic Women: Comparison to Single Energy X-Ray Absorptiometry of the Forearm," Bone, **16**(2), pp. 255–260.
[55] Morris, R. M., Yang, L., Martin-Fernandez, M. A., Pozo, J. M., Frangi, A. F., and Wilkinson, J. M., 2015, "High-Spatial-Resolution Bone Densitometry With Dual-Energy X-Ray Absorptiometric Region-Free Analysis," Radiology, **274**(2), pp. 532–539.